Nanoimprinted diffraction gratings for crystalline silicon solar cells: implementation, characterization and simulation

Alexander Mellor,[1,2,*] Hubert Hauser,[1] Christine Wellens,[1] Jan Benick,[1] Johannes Eisenlohr,[1] Marius Peters,[1] Aron Guttowski,[1] Ignacio Tobías,[2] Antonio Martí,[2] Antonio Luque,[2] and Benedikt Bläsi[1]

[1]*Fraunhofer Institute for Solar Energy Systems ISE, Heidenhofstr. 2, 79110 Freiburg, Germany*
[2]*Instituto de Energía Solar, Universidad Politécnica de Madrid, Avenida Complutense 30, Madrid 28040, Spain*
[*]*alex.mellor@ies-def.upm.es*

Abstract: Light trapping is becoming of increasing importance in crystalline silicon solar cells as thinner wafers are used to reduce costs. In this work, we report on light trapping by rear-side diffraction gratings produced by nano-imprint lithography using interference lithography as the mastering technology. Gratings fabricated on crystalline silicon wafers are shown to provide significant absorption enhancements. Through a combination of optical measurement and simulation, it is shown that the crossed grating provides better absorption enhancement than the linear grating, and that the parasitic reflector absorption is reduced by planarizing the rear reflector, leading to an increase in the useful absorption in the silicon. Finally, electro-optical simulations are performed of solar cells employing the fabricated grating structures to estimate efficiency enhancement potential.

OCIS codes: (040.5350) Photovoltaic; (050.1950) Diffraction gratings

References and links

1. D. Kray and K. R. McIntosh, "Analysis of ultrathin high-efficiency silicon solar cells," Phys. Status Solidi **206**(7), 1647–1654 (2009) (a).
2. P. Sheng, A. N. Bloch, and R. S. Stepleman, "Wavelength-selective absorption enhancement in thin-film solar cells," Appl. Phys. Lett. **43**(6), 579–581 (1983).
3. C. Heine and R. H. Morf, "Submicrometer gratings for solar energy applications," Appl. Opt. **34**(14), 2476–2482 (1995).
4. S. H. Zaidi, J. M. Gee, and D. S. Ruby, "Diffraction grating structures in solar cells," in *Photovoltaic Specialists Conference, 2000. Conference Record of the Twenty-Eighth IEEE* (2000), pp. 395–398.
5. P. Berger, H. Hauser, D. Suwito, S. Janz, M. Peters, B. Bläsi, and M. Hermle, "Realization and evaluation of diffractive systems on the back side of silicon solar cells," in *Proc. SPIE 7725, Photonics for Solar Energy Systems III*, R. B. Wehrspohn, and A. Gombert, eds. (SPIE, Brussels, Belgium, 2010), p. 772504.
6. U. Plachetka, M. Bender, A. Fuchs, B. Vratzov, T. Glinsner, F. Lindner, and H. Kurz, "Wafer scale patterning by soft UV-Nanoimprint Lithography," Microelectron. Eng. **73–74**, 167–171 (2004).
7. H. Hauser, B. Michl, V. Kübler, S. Schwarzkopf, C. Müller, M. Hermle, and B. Bläsi, "Nanoimprint lithography for honeycomb texturing of multicrystalline silicon," Energy Procedia **8**, 648–653 (2011).
8. B. Bläsi, H. Hauser, O. Höhn, V. Kübler, M. Peters, and A. J. Wolf, "Photon Management Structures Originated by Interference Lithography," Energy Procedia **8**, 712–718 (2011).
9. H. Hauser, B. Michl, S. Schwarzkopf, V. Kübler, C. Müller, M. Hermle, and B. Bläsi, "Honeycomb Texturing of Silicon Via Nanoimprint Lithography for Solar Cell Applications," IEEE Journal of Photovoltaics **2**(2), 114–122 (2012).
10. M. Peters, M. Rüdiger, H. Hauser, M. Hermle, and B. Bläsi, "Diffractive gratings for crystalline silicon solar cells—optimum parameters and loss mechanisms," Prog. Photovolt. Res. Appl. **20**(7), 862–873 (2012).
11. L. Zeng, Y. Yi, C. Hong, J. Liu, N. Feng, X. Duan, L. C. Kimerling, and B. A. Alamariu, "Efficiency enhancement in Si solar cells by textured photonic crystal back reflector," Appl. Phys. Lett. **89**(11), 111111 (2006).
12. F. Ning-Ning, J. Michel, Z. Lirong, L. Jifeng, H. Ching-Yin, L. C. Kimerling, and D. Xiaoman, "Design of highly efficient light-trapping structures for thin-film crystalline silicon solar cells," Electron Devices, IEEE Transactions on **54**(8), 1926–1933 (2007).
13. P. Bermel, C. Luo, L. Zeng, L. C. Kimerling, and J. D. Joannopoulos, "Improving thin-film crystalline silicon solar cell efficiencies with photonic crystals," Opt. Express **15**(25), 16986–17000 (2007).

#181212 - $15.00 USD Received 5 Dec 2012; accepted 21 Jan 2013; published 27 Feb 2013

14. S. W. Glunz, "High-efficiency crystalline silicon solar cells," Adv. Optoelectron. **2007**, 97370 (2007).
15. B. Bläsi, H. Hauser, C. Walk, B. Michl, A. Guttowski, A. Mellor, J. Benick, M. Peters, S. Jüchter, C. Wellens, V. Kübler, M. Hermle, and A. J. Wolf, "Photon management structures for solar cells," in *Proc. SPIE 8438, Photonics for Solar Energy Systems IV*, R. Wehrspohn, and A. Gombert, eds. (SPIE, Brussels, Belgium, 2012), pp. 84380Q–84312.
16. A. Mellor, I. Tobías, A. Martí, and A. Luque, "A numerical study of Bi-periodic binary diffraction gratings for solar cell applications," Sol. Energy Mater. Sol. Cells **95**(12), 3527–3535 (2011).
17. A. Mellor, I. Tobías, A. Martí, M. J. Mendes, and A. Luque, "Upper limits to absorption enhancement in thick solar cells using diffraction gratings," Prog. Photovolt. Res. Appl. **19**(6), 676–687 (2011).
18. E. D. Palik, *Handbook of Optical Constants of Solids* (Academic Press, 1997).
19. D. A. Clugston and P. A. Basore, "PC1D version 5: 32-bit solar cell modeling on personal computers," in *Photovoltaic Specialists Conference, 1997., Conference Record of the Twenty-Sixth IEEE* (Anaheim, California, USA, 1997), pp. 207–210.
20. H. Hauser, A. Mellor, A. Guttowski, C. Wellens, J. Benick, C. Müller, M. Hermle, and B. Bläsi, "Diffractive backside structures via nanoimprint lithography," Energy Procedia **27**, 337–342 (2012).
21. E. Schneiderlöchner, R. Preu, R. Lüdemann, and S. W. Glunz, "Laser-fired rear contacts for crystalline silicon solar cells," Prog. Photovolt. Res. Appl. **10**, 29–34 (2002).
22. M. Rüdiger and M. Hermle, "Numerical analysis of locally contacted rear surface passivated silicon solar cells," Jpn. J. Appl. Phys. **51**, 10NA07 (2012).
23. B. Fischer, "Loss analysis of crystalline silicon solar cells using photoconductance and quantum efficiency measurements," in *Physics* (University of Konstanz, Konstanz, 2003).
24. Z. Yu, A. Raman, and S. Fan, "Fundamental limit of nanophotonic light trapping in solar cells," Proc. Natl. Acad. Sci. U.S.A. **107**(41), 17491–17496 (2010).

1. Introduction

Photovoltaic modules employing wafer-based crystalline silicon (c-Si) solar cells currently dominate the solar cell market. The used silicon feedstock accounts for a large part of the module cost. Reducing the volume of silicon used by reducing the solar cell thickness while maintaining the efficiency is therefore considered a key topic in cost reduction. High quality c-Si wafers have been realized with thicknesses in the range of 40 μm and successfully processed into solar cells with over 20% conversion efficiency [1]. Due to the indirect bandgap of c-Si, photons in the wavelength range close to the c-Si band edge (~1.2 μm) are absorbed weakly. This effect is more pronounced for thinner wafers. The use of so called light-trapping schemes to enhance absorption are therefore of increasing importance.

We report on light trapping using rear-side diffraction gratings. In this scheme, the diffraction grating serves to deflect weakly absorbed photons into oblique orders, some of which are confined by total internal reflection at the front surface. This increases their optical path length within the absorber, increasing absorption. Diffraction gratings were first proposed for thin-film solar cells by Sheng *et al.* [2], and later for wafer-based solar cells by Heine and Morf [3]. More recent studies of wafer-based applications can be found in [4, 5].

To be relevant to solar cell production, well defined diffraction gratings must be reproduced on full-wafer areas with high throughput. This can be achieved using nanoimprint lithography (NIL) with interference lithography as the mastering technology [6–8]. NIL has been used to texture c-Si wafers with linear and crossed micron-scale gratings in this work. The process also has up-scaling potential, as shown by a recently developed NIL roller tool [9].

Previous numerical results have shown that the presence of a rear-side grating causes an increase in the photon absorption in the rear reflector [10]. This absorption is parasitic and detracts from the useful absorption in the silicon. In the same reference, it is predicted that this parasitic absorption is decreased if the reflector is planar, as opposed to conformal with the grating texture. To investigate this point, two dielectric buffer layer (DBL) deposition processes have been investigated. One produces a conformal reflector and the other produces a planar reflector. Other authors have proposed distributed Bragg reflectors [11, 12] or three-dimensional photonic crystal back reflectors [13] to prevent reflector absorption. We focus on metal reflectors since they are considered a cheaper solution.

In section 2 of this paper, the details are given of the wafer texturization by NIL, of the two rear-side DBL deposition processes and of the processing of textured wafers into solar cell precursors for optical measurements. In section 3, both the optical and electrical

#181212 - $15.00 USD Received 5 Dec 2012; accepted 21 Jan 2013; published 27 Feb 2013

simulation techniques used to simulate the fabricated structures are described. In section 4, the measured and simulated absorption spectra of all samples are presented. The effect of the rear reflector planarization is discussed and comparison is made between the linear and crossed grating for light trapping. Efficiency enhancements predicted by the combined optical and electrical simulations are presented. In section 5, conclusions are drawn.

2. Experimental details

2.1. Outline of the solar cell precursor structure

Solar cell precursors employing rear-side diffraction gratings were fabricated for optical characterization. These consisted of c-Si wafers coated with a 63 nm thick SiN anti-reflection coating (ARC) on the front side and with a diffraction-grating texture etched into the rear side. Behind the grating was a silicon oxide DBL followed by an Al reflector, this combination is known to provide a good rear reflector [14]. Although this work is ultimately aimed at application to wafers with thicknesses around 40 µm, we have used 200 µm thick monocrystalline silicon wafers in this study, due to availability and ease of handling. A schematic of the solar cell precursor structure is shown in Fig. 1(a).

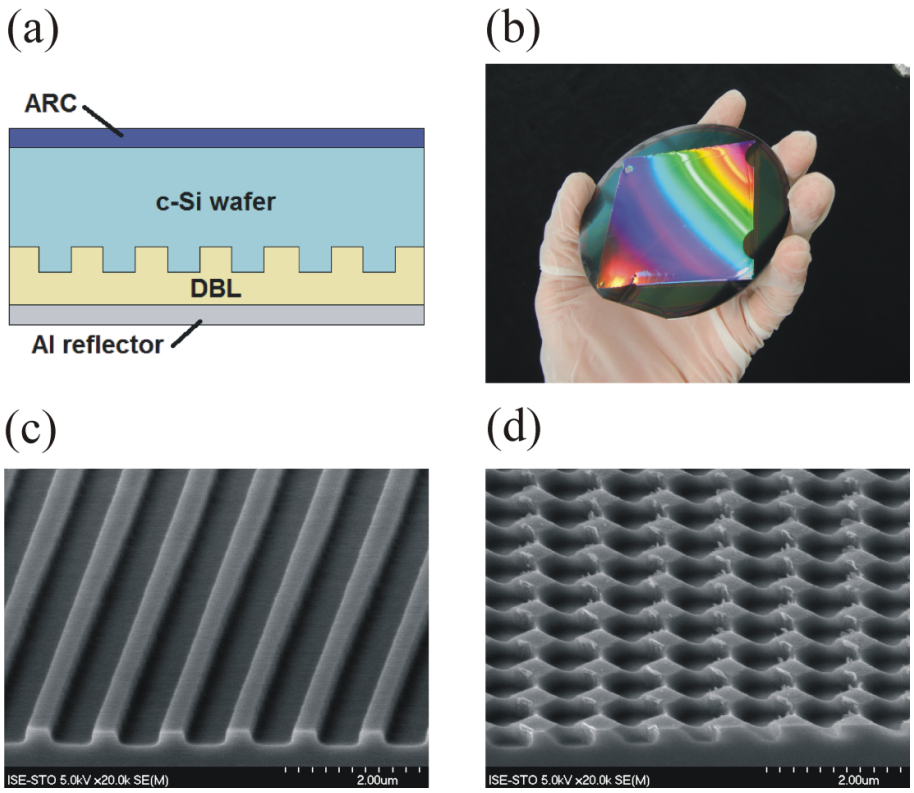

Fig. 1. (a): A schematic diagram of the solar cell precursors fabricated in this work. (b): A photograph of a nanoimprinted linear grating on a 4-inch c-Si wafer. (c) and (d): SEM micrographs of linear (c) and crossed (d) diffraction grating textures in c-Si wafers produced by the described NIL based process chain.

2.2. Nano-texturing of the wafer rear side

The diffraction grating textures were realized on the wafer rear-side by NIL with interference lithography as a mastering technology, followed by reactive ion etching (RIE). This technique allows fine-tailored nanostructures to be realized on large areas with high throughput: a necessity for industrialization. A detailed description of the

#181212 - $15.00 USD Received 5 Dec 2012; accepted 21 Jan 2013; published 27 Feb 2013

process chain can be found in [8, 15]. A brief description is given here. The master structures were realized on glass substrates coated with positive photoresist by two-wave interference lithography followed by a development step. The line grating masters were realized by a single exposure. The crossed grating masters were realized by two exposures with a 90° rotation of the substrate in between. An inverse relief of the master structure was replicated on an addition-curing polydimethylsiloxane (PDMS) stamp by cast molding. The silicon wafer is then coated on the rear side with a low viscosity free-radical curing NIL resist. The stamp was pressed onto the resist and pressure was maintained while the resist was exposed to UV light through the transparent stamp. This left a positive replica of the master structure on the photoresist. The pattern was then transferred into the underlying silicon wafer by RIE. The RIE is strongly anisotropic, favoring etching normal to the wafer plane. The grating depth is determined by the etching time and can be controlled accurately. The photoresist was removed by plasma ashing.

We wished to produce binary gratings with 50% duty cycle. For both the line and crossed gratings, a period of 1 μm was chosen, this having been predicted as the optimum period for 40 μm thick c-Si cells using numerical calculations [10, 16]. The grating depth was 300 nm for the line grating and 200 nm for the crossed grating. These depths had been found to provide the greatest absorption enhancement in preliminary experiments. SEM micrographs of line and crossed gratings etched into the silicon substrates before the DBL deposition are shown in Figs. 1(c) and 1(d) respectively. Figure 1 (b) shows a photograph of a nanoimprinted linear grating on a 4-inch silicon wafer.

2.3. Deposition of the DBL and Al rear reflector

After texturization, the silicon oxide DBL was deposited on the textured surface followed by the thermal evaporation of the Al reflector. We wished to investigate the effect of reflector planarization on the parasitic reflector absorption. The surface profile of the Al reflector is determined by the surface profile of the underlying DBL. Two types of DBL deposition process have therefore been investigated. The first was plasma enhanced chemical vapor deposition (PECVD). In this vapor phase process, a layer of SiO_2 is deposited conformally with the surface texture, causing the subsequently deposited Al reflector to be conformal with the grating. The second technique was deposition of a dispersion of colloidal silica nanoparticles onto the textured surface by spin coating, which later dried in air. This liquid phase process leaves a layer with a planar surface even when the underlying substrate is textured. The Al reflector is then grown on this surface. Preliminary experiments were made to deposit a SiO_2 layer on textured photoresist-on-glass substrates by spin coating with the aim of achieving a flat surface. The result is shown in Fig. 2.

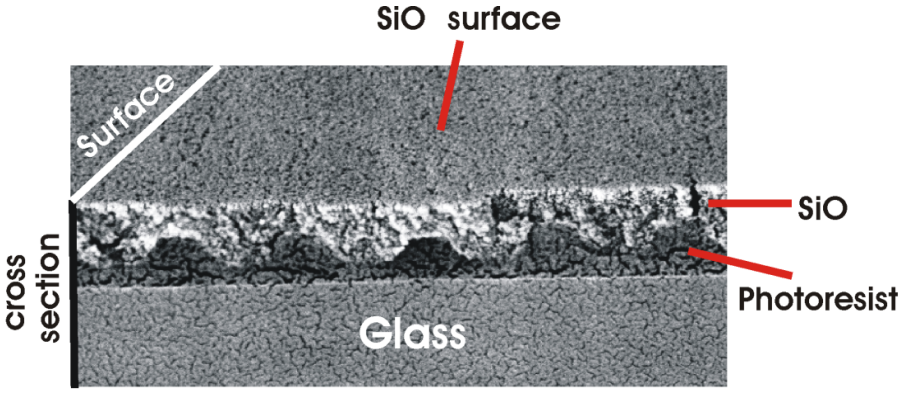

Fig. 2. A planar SiO layer deposited on a textured photo-resist-on-glass substrate via spin coating.

The rear of solar cell precursors with linear diffraction gratings employing the PECVD DBL and spin-coated DBL are shown in Figs. 3(i) and 3(ii) respectively. The

#181212 - $15.00 USD Received 5 Dec 2012; accepted 21 Jan 2013; published 27 Feb 2013

PECVD technique clearly produces a reflector that is conformal with the diffraction grating. The spin-coating technique has not produced a perfectly planar reflector, as had been expected, but a slightly modulated one. This is despite the silicon oxide surface being planar before Al deposition. We attribute this to thermally induced densification of the nanoporous silicon oxide layer during the aluminium evaporation process, during which surface temperatures in the range of 200°C can be expected. Nonetheless, the Al surface is clearly more planar for the spin-coating method than for the PECVD method. The effect of imperfect reflector planarization on the parasitic absorption is investigated in Section 4.

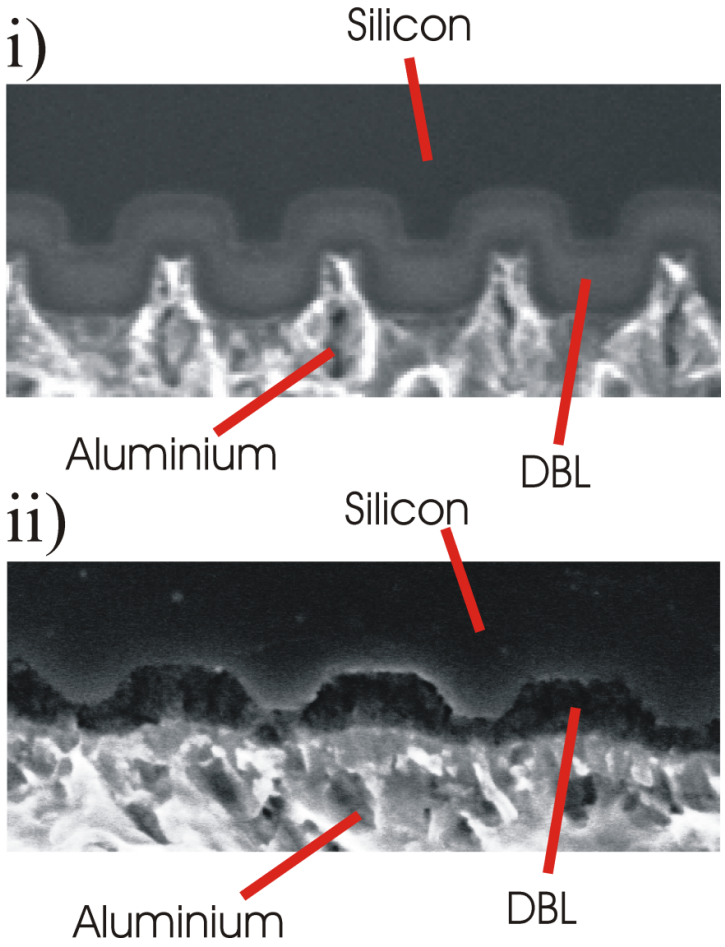

Fig. 3. SEM micrographs of the cross section of the rear side of two solar cell precursors with linear grating textures. (i): DBL deposited by PECVD. (ii): DBL deposited by spin-coating.

2.4. Summary of fabricated samples

Solar cell precursors where fabricated with rear-side linear and crossed grating textures. The PECVD DBL deposition technique was applied to both a linear and a crossed grating structure. The spin-coated oxide layer was only applied to a linear grating structure. A planar reference was also fabricated. This consisted of a 200 µm thick crystalline silicon wafer with a 63 nm SiN ARC on the front side and a 500 nm thick PECVD SiO_2 DBL followed by an Al reflector on the rear side. Table 1 shows the relevant information for each sample. The rear sides of samples B and C are those pictured in Figs. 3(i) and 3(ii) respectively.

#181212 - $15.00 USD
Received 5 Dec 2012; accepted 21 Jan 2013; published 27 Feb 2013

Table 1. Grating Type and DBL Deposition Technique for Each Sample

Sample name	Grating type	DBL deposition technique
ref	no grating	PECVD
A	crossed	PECVD
B	linear	PECVD
C	linear	Spin-coating

2.5. Optical characterization

The wavelength dependent absorption of all solar cell precursors was measured by reflection spectroscopy using a Fourier transform spectrometer and an integrating sphere. The absorption was calculated by *Absorption = 1 – Reflection*, under the assumption that there is zero transmission through the 2 μm thick Al reflector.

3. Simulation techniques

3.1. Optical simulation technique

The measured absorption from the optical characterization is the sum of the useful absorption in the silicon and the parasitic absorption in the reflector. Optical simulations of the fabricated solar cell precursors were therefore performed, allowing the absorption in the silicon and in the aluminium to be calculated explicitly. The optical simulation technique used is that presented in [17]. The diffraction-grating region is simulated wave-optically using rigorous coupled wave analysis (RCWA) to yield a far-field intensity scattering matrix. This is combined with a simple steady state matrix formalism, which describes the propagation of the diffracted orders within the silicon bulk. The orders in the bulk are treated incoherently. This is a good approximation for structures whose absorber thickness is more than an order of magnitude greater than the coherence length of the incident light (~1μm for solar illumination). The complex refractive indices of all materials used are taken from the literature [18] or have been obtained by ellipsometry measurements. For all simulations, we have assumed normal incidence by a cone of light of apex half-angle 0.26°, corresponding to direct on-axis solar illumination without concentration.

3.2. Electrical simulation technique

To estimate the efficiency enhancements that would be achieved if the fabricated solar cell precursors were further processed into solar cells, optically simulated depth dependent photogeneration profiles were used as input parameters for PC1D simulations [19]. For each grating structure, the depth dependent current generation in the cell is calculated using the simulation technique described in the previous section.

Relevant cell parameters for the solar cell simulations were: p-type 1 Ωcm material with a bulk minority carrier lifetime of 1 ms; a Gaussian shaped 120 Ω/□ emitter with a peak doping density of $1x10^{19}$ cm^{-3} and a junction depth of 1 μm; an effective front surface recombination velocity of 1000 cm/s. Shading losses due to front side metallization were not considered within this work.

It has been assumed that the impact of the grating on the electrical parameters can be described by adjusting the effective rear surface recombination velocity (S_{back}). Typically, texturing of the silicon wafer leads to increased S_{back} due to surface enlargement and plasma damage. Recently, a solar cell structure was presented in which the diffraction grating is electrically insulated from the electrically active region [20]. This was achieved by depositing a thin layer of Al_2O_3 on the un-textured rear side of the Si wafer by atomic layer deposition, followed by an amorphous silicon (a-Si) layer. The a-Si layer was then textured using the same NIL process used in this work, producing a diffraction grating that is electrically isolated from the solar cell. Lifetime measurements showed the recombination velocity of the passivated rear surface (S_{pass}) to be as low as 11cm/s after texturing, as opposed to 8 cm/s before.

We assume the rear of the solar cell to be metalized via laser-fired-contacts (LFC [21]). We therefore calculate an effective S_{back} based on the assumptions and

#181212 - $15.00 USD Received 5 Dec 2012; accepted 21 Jan 2013; published 27 Feb 2013

optimizations described in [22]. The most important assumptions are a contact pitch of 800 μm (optimized for 1 Ωcm material and 200 μm wafer thickness) and a contact radius of 45 μm leading to a metallized fractional area of 1%. The surface recombination velocity for the metallized areas was determined to be $11.3x10^3$ cm/s, also according to [22], and the remaining area was taken to have a surface recombination velocity of S_{pass} described in the previous paragraph (11cm/s for the textured cells and 8 cm/s for the reference cell). These values were then used as input for the equation introduced in [23] to calculate an effective S_{back} . The resulting values for the effective S_{back} were 61 cm/s and 64 cm/s for 200 μm thick wafers with the planar and the textured rear respectively. For 40 μm thick wafers, the same model was applied, leading to corresponding values of 69 cm/s and 72 cm/s.

3.3. The simulated structures

The simulated geometries are shown in Fig. 4. The geometries for A and B and C have been deduced from SEM images of the respective samples. The slightly modulated reflector of sample C (see Fig. 3(ii)) has been included in the simulated structure (Fig. 4(c)). To investigate the effect of this slight modulation, and to predict what can be achieved if the reflector were further planarized, an additional geometry has been simulated, which is identical to sample C, but has a perfectly planar reflector. This is labeled sample D, and is shown in Fig. 4(d). It is stressed that sample D is purely theoretical and does not represent a structure that has actually been fabricated in this work.

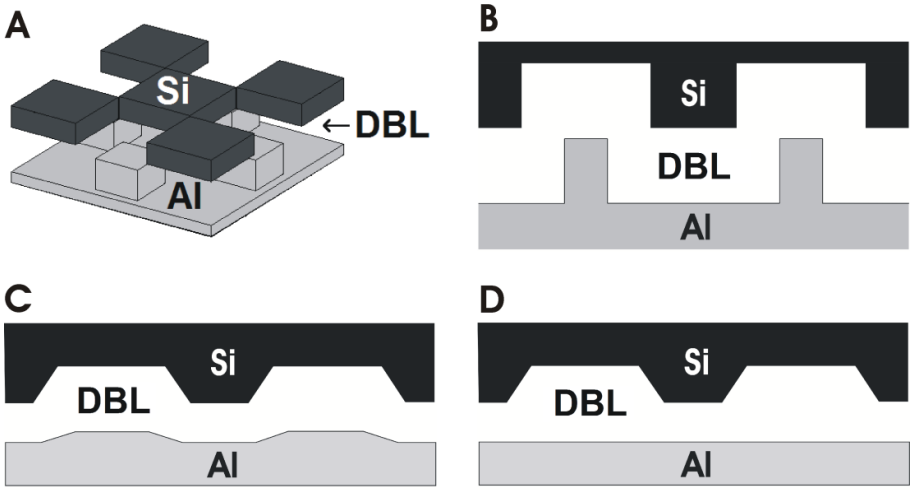

Fig. 4. The simulated geometry for each grating structure. Each image is labeled with the corresponding sample name. In A, the transparent layer between the Si and the Al represents the DBL.

4. Results and discussion

4.1. Measured and simulated absorption spectra

The absorption is shown for each sample in Fig. 5. The red circles show the measured total absorption and the black curves show the simulated total absorption. Only the wavelength range for which an appreciable number of photons reach the gratings has been plotted. Good agreement is observed between the measured and simulated total absorption. This gives confidence in the simulations as a tool for quantitative analysis.

The simulated absorption has been decomposed into the useful Si Absorption and the parasitic Al absorption; these are respectively the green and blue curves in Fig. 5. To summarize this data, the following absorbed photocurrent densities have been calculated and are given for each sample in the insets of the figure.

#181212 - $15.00 USD Received 5 Dec 2012; accepted 21 Jan 2013; published 27 Feb 2013

$$j_{ph,Si} = q_e \int \Phi_{Am1.5G} abs_{Si} d\lambda$$
$$j_{ph,Al} = q_e \int_{\lambda<1.2\mu m} \Phi_{Am1.5G} abs_{Al} d\lambda \quad (1)$$

where $\Phi_{Am1.5G}$ is photon flux of the Am1.5G spectrum, q_e is the elementary charge, and abs_{Si} and abs_{Al} are respectively the absorption in the Si and Al. The $j_{ph,Si}$ is the useful absorbed photocurrent density and represents the upper limit for the j_{sc}, which would be achieved if all photo-generated carriers were to reach the external contacts. The $j_{ph,Al}$ is simply the number of photons that are absorbed in the aluminium expressed as a current density for ease of comparison. Only photons with energy above the c-Si band edge are included in the latter calculation.

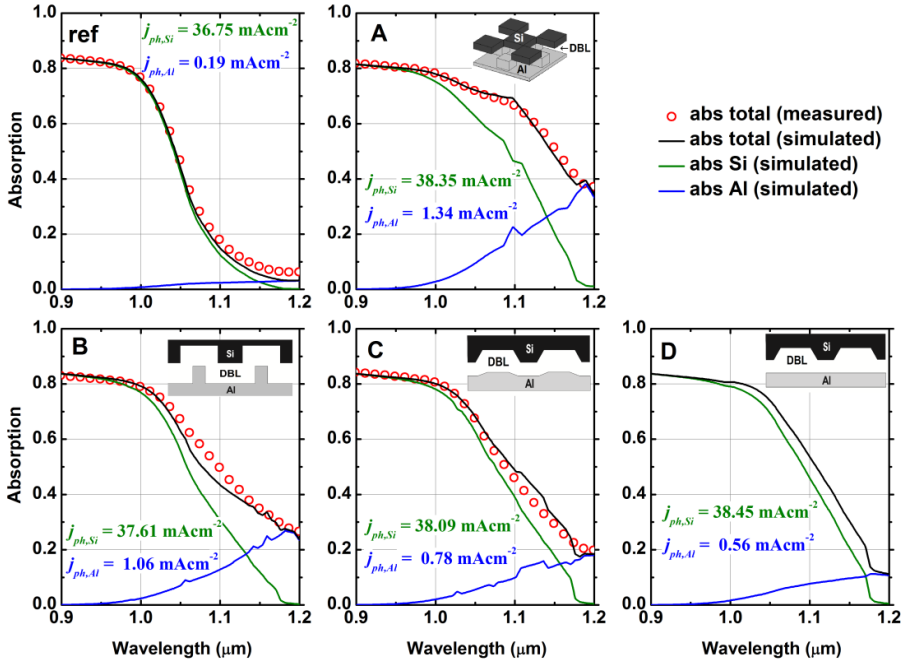

Fig. 5. Absorption spectra for the solar cell precursors employing the grating structures. The structure name is shown in the top left of each graph. Red circles show the measured total absorption, black curves show the simulated total absorption, green curves show the simulated silicon absorption, and blue curves show the simulated aluminium absorption. The calculated $j_{ph,Si}$ *and* $j_{ph,Al}$ for each structure is shown in the inset of each graph.

Both the measured and simulated results show that the diffraction gratings provide significant absorption enhancements in the wavelength range of interest, compared to the reference. Samples A and B respectively have crossed and linear gratings; however, they are otherwise equivalent in that the gratings are binary with a deep binary modulation in the reflector. Sample A has a higher $j_{ph,Si}$ than sample B; this supports previous theoretical predictions that bi-periodic gratings are better for light trapping than uni-periodic gratings [17, 24]. However, Sample A also has a higher $j_{ph,Al}$ than sample B; this suggests that the advantage of a bi-periodic grating is somewhat mitigated by an increased parasitic absorption. This could be because, for the bi-periodic grating, a greater number of orders are excited in the DBL and because photons with both TE and TM polarizations are more effectively coupled into the reflector.

Comparing sample C with sample B, the simulations suggest that the reflector planarization achieved using the spin-coating DBL deposition method does indeed cause a reduction in the parasitic absorption and consequently an increase in the useful silicon

#181212 - $15.00 USD Received 5 Dec 2012; accepted 21 Jan 2013; published 27 Feb 2013

absorption. The results for sample D suggest that this could be improved if the novel deposition process were developed further to achieve a perfectly planar reflector.

To increase confidence in the simulated results, the polarization dependent reflection spectrum has been measured and simulated for sample B. This is shown in Fig. 6. Good agreement is achieved between the measured and simulated reflection spectra. Particularly, both measurement and simulation show that TE absorption is stronger than TM absorption for $\lambda < 1.1$ μm, where the Si absorption is dominant; whereas TM absorption is stronger than TE absorption for $\lambda > 1.1$ μm, where the Al absorption is dominant. This suggests that the simulation technique is calculating both the Si and Al absorption accurately. It should be mentioned that the spectrometry measurement was taken with an incident-beam angle of 8°, whereas the simulation assumed normal incidence.

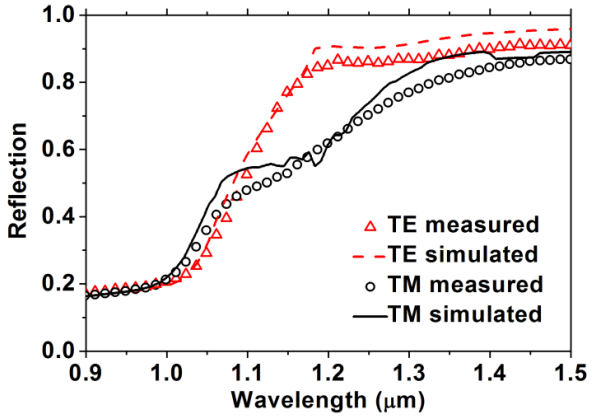

Fig. 6. The measured and simulated polarization dependent reflection spectrum for Sample B. TE refers to transverse electric and TM to transverse magnetic polarization.

4.2. Simulated IV characteristics and efficiencies

The predicted IV characteristics for 200 μm thick and 40 μm thick solar cells are presented in Tables 2 and 3 respectively. In each case, the absorption profile has been calculated as described in Section 3.1 and the IV characteristics have been calculated as described in Section 3.2. The absolute efficiency enhancement refers to the difference between each grating-equipped cell and the reference. Results are not presented for sample D, since it is based on a structure that has not been fabricated in this work. The efficiencies have to be seen as upper limit for the given j_{sc} and V_{oc} values, since ideal cell parameters for series and parallel resistances were assumed, leading to an ideal fill factor of around 84%. Structure A — the crossed grating — gives the highest efficiency enhancement for both cell thicknesses. Furthermore, it can be seen that the absolute gain in efficiency is more pronounced for the 40 μm thick cells; a maximum gain of 1.6% absolute can be achieved under the given assumptions. What's more, the high values for V_{oc} for all samples indicate that the introduction of a rear side grating is not necessarily related to degraded electrical characteristics.

Table 2. Predicted IV Characteristics of 200 μm Thick c-Si Solar Cells Employing Each Grating Structure

Structure Name	j_{sc} (mAcm^{-2})	V_{oc} (mV)	η (%)	$\Delta\eta$ (%)
Ref	36.5	685.8	21.1	
A	38.0	686.1	22.0	0.9
B	37.3	685.7	21.6	0.5
C	37.8	685.9	21.9	0.8

j_{sc}: short circuit current density, V_{oc}: open circuit voltage, η: efficiency, $\Delta\eta$: absolute efficiency enhancement compared to planar reference.

#181212 - $15.00 USD Received 5 Dec 2012; accepted 21 Jan 2013; published 27 Feb 2013

Table 3. Predicted IV Characteristics of 40 µm Thick c-Si Solar Cells Employing Each Grating Structure

Structure Name	j_{sc} (mAcm^{-2})	V_{oc} (mV)	η (%)	$\Delta\eta$ (%)
Ref	33.7	686.2	19.5	
A	36.4	687.2	21.1	1.6
B	35.0	686.4	20.3	0.8
C	35.9	686.9	20.8	1.3

Symbols as defined in Table 2

5. Conclusions

Monocrystalline silicon (c-Si) wafers have been textured with diffraction gratings using NIL with interference lithography as the mastering technology. Both linear and crossed gratings have been produced with binary profiles, close to 50% duty cycles, 1 µm periods and depths of a few hundred nanometers. Dielectric buffer layers and rear reflectors have been deposited on the textured surface, comprising an effective rear-side light trapping structure for solar cells. Two deposition techniques have been employed to apply a dielectric buffer layer between grating and reflector: a conventional PECVD method and a method consisting in spin-coating of a dispersion of colloidal SiO_2 nano-particles. The former causes the subsequently deposited reflector to be conformal with the grating texture and the latter causes it to be planar.

Solar cell precursors employing the grating structures have been fabricated and the absorption has been measured by reflection spectroscopy. Optical simulations of the fabricated structures have also been performed, allowing the total absorption to be decomposed into useful absorption in the silicon and parasitic absorption in the rear reflector. Excellent agreement is observed between the measured and simulated absorption spectra. Significant absorption enhancements are observed for the grating structures compared to the planar reference. The crossed grating is shown to provide better absorption enhancement than the equivalent linear grating. The grating with a planarized reflector is shown to cause a lower parasitic absorption and higher useful absorption than the grating with the conformal reflector.

The efficiency potential of the fabricated solar cell precursors has been estimated using a PC1D simulation. The depth dependent photogeneration determined using the optical simulations of the fabricated grating geometries were used as input parameters. Measured values for the passivated rear surface recombination velocity were used to estimate the effective rear surface recombination velocity of a locally contacted cell. As a result of these simulations, it can be concluded that the introduction of such a photonic structure on the wafer rear can be achieved and still excellent values for the open circuit voltage can be expected. The gain in the short circuit current density for the crossed gratings leads to efficiency enhancements of up to 0.9% and 1.6% absolute for 200 µm and 40 µm thick wafers with planar front respectively.

Acknowledgments

Parts of this work were funded by the German Federal Ministry of Environment, Nature Conservation and Nuclear Safety under contract numbers 0325176 (NanoTex) and 0329849A (ThETA), the German Federal Ministry of Education and Research under contract number 03SF0401 (InfraVolt), the EC through the project NGCPV (Grant No. 283798) and the Comunidad de Madrid through the project NUMANCIA2 (Grant No. S2009/ENE1477). Alexander Mellor gratefully acknowledges the Comunidad de Madrid for financial support through the scholarship Personal Investigador de Apoyo.